

HYDROCARBON MICROTREMORS INTERPRETED AS NONLINEAR OSCILLATIONS DRIVEN BY OCEANIC BACKGROUND WAVES

R. Holzner, P. Eschle, S. Dangel

Spectraseis Technologie AG, Zurich, Switzerland

M. Frehner

Department of Earth Sciences, ETH Zurich, Switzerland

C. Narayanan, D. Lakehal

ASCOMP GmbH, Zurich, Switzerland

Submitted on 19 December 2006 to

topical issue "Geophysics" of

COMMUNICATIONS IN NONLINEAR SCIENCE AND NUMERICAL SIMULATION

as a follow up of presentations given at the conference on

NONLINEAR DYNAMICAL METHODS AND TIME SERIES ANALYSIS,

Udine , Italy, 30 August - 1 September, 2006

Abstract

Characteristic low frequency seismic signals have been observed in areas where hydrocarbon reservoirs are present. A possible interpretation is the excitation of hydrocarbon related resonances. Basic models of an oscillating liquid filled porous medium are investigated. Synthetic spectra of the ab initio Navier-Stokes equations and of basic linear and non-linear one-dimensional oscillators show characteristic features of measured spectra when oceanic background waves around 0.1 - 0.2Hz are assumed to be the external driving force.

Introduction

Hydrocarbon Microtremor Analysis (HyMAS) [1,2] is an innovative seismic spectroscopy technology identifying the hydrocarbon content of geological structures by analyzing low frequency background wave signals. Hydrocarbon indicating information is extracted from spectral modifications of naturally occurring background waves in the 0.1 – 20 Hz range interacting with hydrocarbon bearing porous structures. Similar observations have been made at more than 15 sites worldwide

[3,4,5,6]. From recent land surveys in Austria and Brazil [1,7] typical HyMAS data of a weak and a strong signal indicating low and high hydrocarbon potential are shown in Fig. 1.

A general approach towards an explanation of such behaviour is the phenomenological interpretation as a driven linear or non-linear oscillator [8].

The straight forward approach to describe such observations is the general equation for a one dimensional nonlinear oscillator

$$\frac{\partial^2 x}{\partial t^2} + \frac{b}{m} \frac{\partial x}{\partial t} + \omega_0^2 x(1 + Ax + Bx^2) = \frac{F}{m} \sin(\Omega t) \quad (1)$$

with space variable x , frictional damping term b/m , resonance frequency ω_0 , driving acceleration amplitude F/m and driving frequency Ω , which already leads to a remarkably good fit as displayed in Fig. 1. The input excitation F/m at the ocean wave peak frequency of $\Omega = 2\pi \cdot 0.22$ Hz generates a second harmonic at about 0.44 Hz. The resonance frequency, which was intentionally set to $\omega_0 = 2\pi \cdot 2.6$ Hz, has been widened by the creation of sum- and difference frequencies between Ω and ω_0 the damping term b/m .

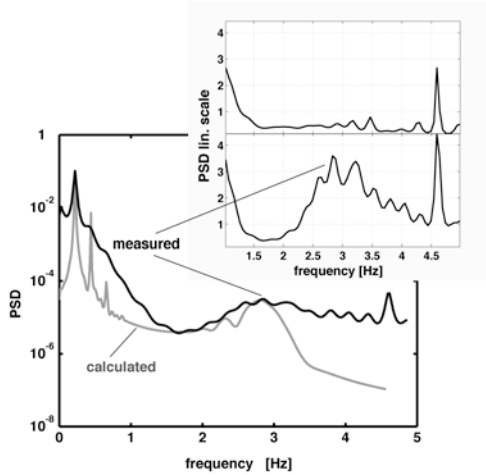


Figure 1: Spectrum (calculated) produced by a driven nonlinear one-dimensional oscillator which compares well with the measured spectrum of the vertical ground motion velocity component. For comparison the maximum values of the spectra are superimposed and set to a value close to one. Parameters for the calculations according to Eq. 1 are : $b/m = 2.0 \text{ s}^{-1}$, $\omega_0 = 2 \cdot \pi \cdot 2.6 \text{ Hz}$, $F/m = 0.8 \text{ m s}^{-2}$, $\Omega = 2 \cdot \pi \cdot 0.22 \text{ Hz}$, $A/\omega_0^2 = 1.2 \cdot 10^4 \text{ s}^{-2}$, $B/\omega_0^2 = 4 \cdot 10^5 \text{ s}^{-2} \text{ m}^{-1}$.

The insert shows the measured signal after suitable signal to noise ratio improving data processing. The trace on top indicates low and the trace at the bottom high hydrocarbon potential. The measurement locations were about 2 km apart. The peak at about 4.5 Hz is due to a nearby artificial noise source.

Note that the frequency separation of the clearly visible fine structure wiggles corresponds to the frequency of the oceanic wave peak which is likely to be caused by non-linear interactions. Also the higher harmonics of the driving frequency are visible in the measured spectrum.

In order to better understand the meaning of such formal results and their limits, the oscillator parameters and the conditions of the natural environment of a hydrocarbon reservoir have to be related. Two basic poromechanical models often used in literature serve as examples [9]. For the linear model (Fig. 2), a bi-conical pore geometry (Fig. 3) is used while a spherical pore shape (Fig. 12) represents the nonlinear case.

Linear one dimensional oscillator model

The bi-conical pore geometry has the advantage of providing a linear spring

constant for the restoring force which is independent of the dislocation of the pore fill along the z-direction. In equilibrium, the capillary forces which are proportional to the length of the oil/rock contact line (ORCL) balance each other.

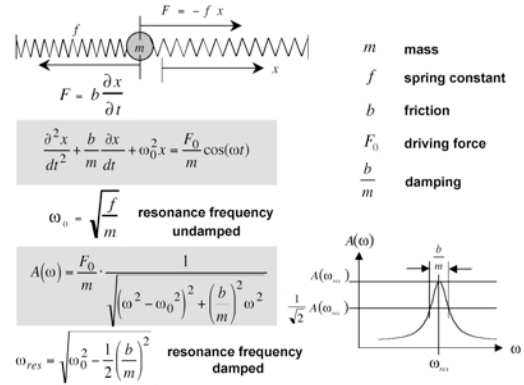


Figure 2 : General description of a driven linear one-dimensional oscillator along the x -direction with its second order differential equation and resonance response function.

For small displacements of the liquid, the lengths of both ORCL change in such a way that the related capillary forces $F_z = F_{+z} + F_{-z}$ always add up to a restoring force which enables oscillations.

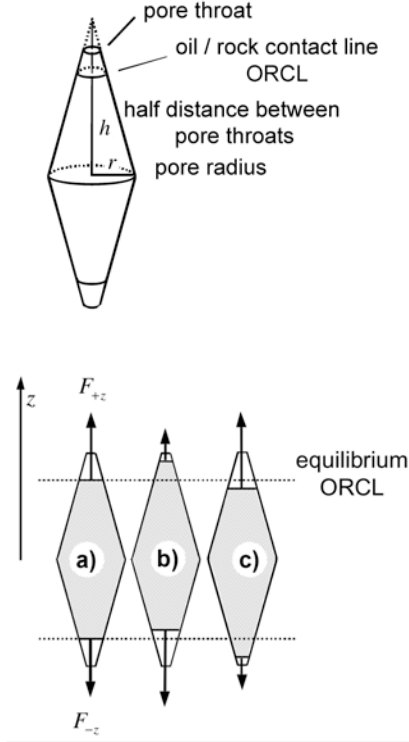


Figure 3: Schematic representation of a simple bi-conical pore geometry which enables low frequency oscillations of the contained liquid along the z-direction. The oil/rock contact line (ORCL) or triple phase line where capillary forces occur is formed between the oil and water phases and the rock material. a) liquid in equilibrium: the capillary forces F_{+z} in positive and F_{-z} in negative z-direction balance each other; b) Situation after a small displacement of the liquid in the positive z-direction: F_{+z} has decreased and F_{-z} has increased compared to the equilibrium. The resulting restoring force drives the liquid back along the negative z-direction towards its equilibrium position; c) same as b) with dislocation in the negative z-direction.

Neglecting gravity, which would mainly shift the equilibrium position, and assuming nearly filled pores, an oscillation frequency according to the one-dimensional oscillator model can be estimated.

The spring constant

$$f = \frac{\partial F_z}{\partial z} = \gamma \frac{2\pi r}{h} \quad (2)$$

and mass

$$m = \frac{2}{3} r^2 \pi h \rho_L \quad (3)$$

lead to the resonance frequency

$$\nu = \frac{1}{2\pi} \sqrt{\frac{f}{m}} = \frac{1}{2\pi h} \sqrt{\frac{6\gamma}{r \rho_L}} \quad (4)$$

The observed value of $\nu = 3$ Hz is compatible with realistic values of the relevant parameters given in Tab. 1.

pore radius	r	$1 \cdot 10^{-3}$	m
half distance between pore throats	h	$5 \cdot 10^{-3}$	m
surface tension of oil	γ	10^{-3}	N m ⁻¹
density of oil	ρ_L	$8 \cdot 10^2$	kg m ⁻³
viscosity	μ	$6 \cdot 10^{-4}$	kg s ⁻¹ m ⁻¹
low viscosity	μ	$6 \cdot 10^{-5}$	kg s ⁻¹ m ⁻¹
resonance frequency	ω_0	$3 \cdot (2 \cdot \pi)$	Hz

Table 1: common parameter values

Fig. 4 shows, as an example, how the sharp-peaked spectrum of a single oscillator approaches the wider observed shape as a function of the width "sigma" of the assumed log-normal parameter distribution.

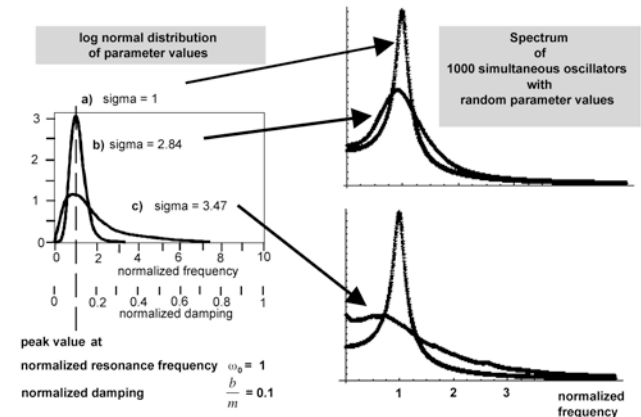


Figure 4: Numerical simulation of the superimposed spectrum of 1000 linear harmonic oscillators for three different parameter distributions: a) all oscillators with normalized resonance frequency at $\omega_0=1$ and damping $b/m=0.1$; b) both resonance frequency and damping

vary according to a log-normal distribution with sigma = 2.84; c) both resonance frequency and damping vary according to a broad log-normal distribution with sigma = 3.47.

Navier-Stokes equations

In order to verify the approximations used in the one-dimensional oscillator model, the Navier Stokes equations which are mainly based on fundamental ab initio concepts such as conservation laws, constitutive equations and boundary conditions for the liquid filled bi-conical pore are numerically solved.

Code

TransAT [10] is a finite-volume multi-physic code solving the multi-fluid Navier-Stokes equations. The code uses multi-block, structured meshes along with a message-passing parallel algorithm. The grid arrangement is collocated and can handle general curvilinear grids. Multiphase flows are computed using the particle tracking approach, or interface tracking techniques. The flow is modeled as one fluid having variable material properties according to a phase indicator function which distinguishes the gas phase regions from the liquid phase. Both the Level-Set and the Volume-of-Fluid Interface Tracking Methods (ITM) can be employed in the code to track evolving interfaces.

Transport Equations

The incompressible heat and fluid flow equations expressed within the single-fluid formalism take the following form

$$\nabla \cdot \mathbf{u} = 0 \quad (5)$$

$$\partial_t(\rho \cdot \mathbf{u}) + \nabla \cdot (\rho \cdot \mathbf{u} \cdot \mathbf{u} - \boldsymbol{\sigma}) = F_s + F_b + F_u \quad (6)$$

where ρ is the density of the liquid pore fill, \mathbf{u} is the velocity vector of the pore fill and the RHS terms in the momentum equation (Eq. 6) represent the surface tension expressed by Eq. 8 below, body forces and the triple-line wall contribution respectively and $\boldsymbol{\sigma} = \boldsymbol{\tau} - p \cdot \mathbf{I}$ is the Newtonian viscous stress tensor with its

share component $\boldsymbol{\tau}_w$ parallel to the wall and its pressure induced component $p \cdot \mathbf{I}$ (p : pressure, \mathbf{I} : identity matrix). Isothermal conditions are assumed.

The Level Set Method

In the LS method, the interface between immiscible fluids is represented by a continuous function ϕ , representing the distance to the interface which is positive on one side and negative on the other. The two fluids can now be identified by the location of the interface representing the zero level. The LS evolution equation is

$$\partial_t \phi + \mathbf{u} \cdot \nabla \phi = 0 \quad (7)$$

Material properties such as the density, the viscosity, and the thermal conductivity are updated locally based on ϕ and smoothed across the interface using a smooth Heaviside function. The fact that ϕ is a continuous function across the interface helps to determine the normal vector \mathbf{n} to the interface, and thereby the surface curvature κ required for the determination of the surface tension,

$$F_s = \gamma \kappa \delta_s \mathbf{n} \quad (8)$$

where γ is the surface tension of the fluid and δ_s is the Dirac delta function located at the interface.

Simulation setup and results

The bi-conical pore is setup as an axisymmetric body of revolution as shown in Fig. 5. The pore is initialised with oil in the center and water at the edges. A sinusoidal forcing is applied to the flow domain of given amplitude (0.05 mm) and frequency. The simulation is run for a fixed number of cycles and the motion of the center-of-mass of the oil is calculated. By comparing the amplitude and phase of the oscillation with the imposed oscillation, the amplitude and phase response of the system is computed.

Two pores with center diameter of 3mm and 1mm were simulated for a range of frequencies (0.5 – 10 Hz). Further refinement in the frequencies was performed near the observed resonance frequency for the 3mm diameter case. Fig. 6 shows the amplitude and phase response for the 3 mm diameter pore. Resonance is observed at approximately 1 Hz for a viscosity of $\mu=6\cdot 10^{-4}$ kg s⁻¹ m⁻¹. For a lower viscosity ($\mu=6\cdot 10^{-5}$ kg s⁻¹ m⁻¹) the resonance frequency is shifted to approximately 1.7 Hz. As expected the phase angle undergoes a 90 degree shift at resonance. For the 1mm pore, resonance is observed at approximately 4.6 Hz (Fig. 7).

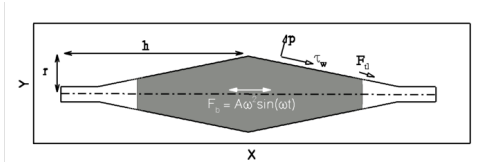


Figure 5: Bi-conical pore geometry with forces acting on the oil drop. For the calculations two pore shapes with of $r=1$ mm, $h=1.5$ mm and $r=3$ mm, $h=4.5$ mm were used. The external force was adjusted for a non resonant displacement of $A=2\cdot 10^{-6}$ m for the 1 mm pore diameter and of $A=2\cdot 10^{-5}$ m for the 3 mm pore diameter.

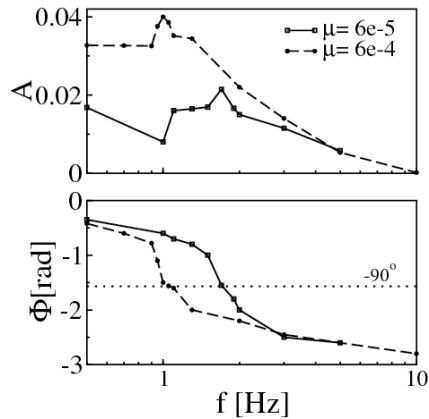


Figure 6: Amplitude A (mm) and phase response Φ (rad) for 3mm pore diameter. Viscosity $\mu=6\cdot 10^{-4}$ kg s⁻¹ m⁻¹ and $\mu=6\cdot 10^{-5}$ kg s⁻¹ m⁻¹

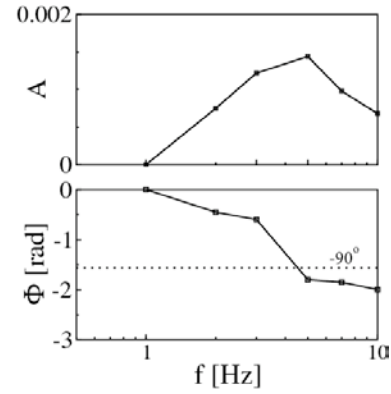


Figure 7: Amplitude A (mm) and phase response Φ (rad) 1mm pore diameter. $\mu=6\cdot 10^{-4}$ kg s⁻¹ m⁻¹

Forces acting on the oil drop

The different forces acting on the oil drop at two different frequencies (1 Hz and 3 Hz) for the 3 mm pores are shown in Figs. 8(a) and (b). The forces acting on the oil drop are schematically shown in Fig. 5, namely the wall pressure and viscous shear, the inertial force, the triple line force at the ORCL, the surface tension force, and the imposed sinusoidal oscillation. Different forces have different amplitude and phase relationships to the imposed oscillation. The wall pressure is typically in phase with the imposed oscillation, whereas the viscous shear lags the imposed oscillation.

The variation of the magnitudes of the different forces with respect to the imposed frequency normalised by the imposed oscillation magnitude is shown in Fig. 9. It can be observed that the forces generally reduce with increasing frequency. They also show a small increase/decrease in amplitude near the resonance frequency (approximately 1 Hz).

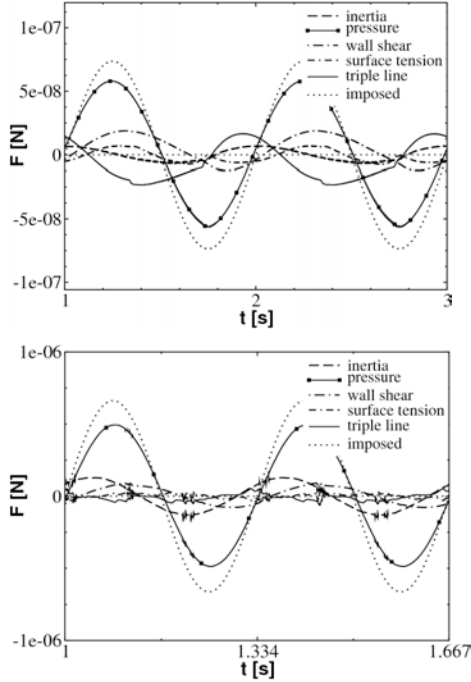


Figure 8(a): Forces acting at 1 Hz on oil drop, **(b):** Forces acting at 3 Hz on oil drop. The little bursts are numerical oscillations due to the contact line moving from one finite volume to another. Special treatment is done only on one control volume for the dynamic contact line model.

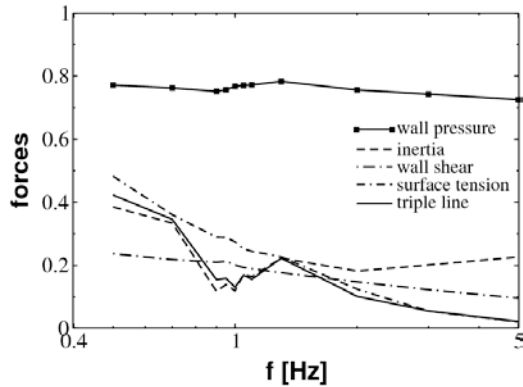


Figure 9: Variation of forces with respect to frequency. The forces add up to one considering that the triple line force is a negative contribution and the surface tension force is an internal force of which the resulting net force is represented by the triple line force.

Comparison of calculated pore oscillation behaviour to a linear harmonic oscillator

Fig. 10 shows the frequency dependence of amplitudes and phases calculated by the numerical Navier-Stokes model (NSM) and the linear harmonic oscillator model (LHOM) for 3 cases : pore of 1mm radius and 3mm radius with two different viscosities. For each case two fits are indicated, one for good agreement in the maximum amplitude region and one for good agreement at frequencies far below and above resonance. The oscillator parameters for each case and fit are listed in Tab. 2.

The expressions for the response of a linear harmonic oscillator are

$$A(\omega) = \frac{F_0}{m} \frac{1}{\sqrt{(\omega_0^2 - \omega^2)^2 + \left(\frac{b}{m}\right)^2 \omega^2}} \quad (9)$$

for the amplitude and

$$\Phi = -\arctan\left(\frac{\frac{b}{m}\omega}{\omega_0^2 - \omega^2}\right) \quad (10)$$

for the phase with excitation acceleration $\frac{F_0}{m}$, resonance frequency ω_0 and damping $\frac{b}{m}$.

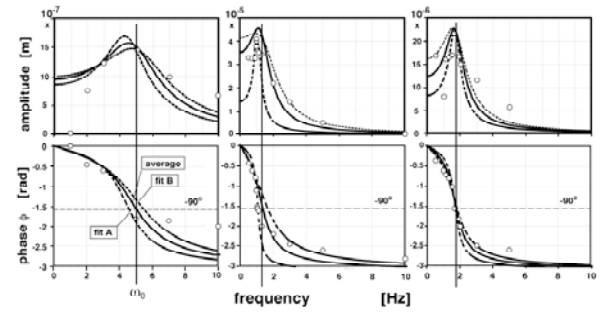


Figure 10 : Amplitudes and phases calculated by the Navier-Stokes model (NSM) and the linear harmonic oscillator model (LHOM) for a pore of 1mm radius (left) and 3mm radius (middle : same viscosity as 1mm pore; right: lower viscosity). Open circles : calculated by NSM; fit A dashed line: LHOM fitted for good agreement around the resonance frequency; fit B dashed line: LHOM fitted for good agreement at the wings; solid line: average of fit A and fit B.

	1mm pore radius			3mm pore radius			3mm pore radius low viscosity		
	fit B	fit A	average	fit B	fit A	average	fit B	fit A	average
excitation [10 ² m s ⁻²]	3	1.8	2.4	12	1.7	6.85	5.5	2.5	4.0
resonance frequency [Hz]	5.5	4.6	5.05	1.7	1.1	1.4	1.85	1.75	1.8
damping [s ⁻¹]	2.0	1.2	1.6	1.0	0.18	0.59	0.7	0.32	0.51

Table 2 : Harmonic oscillator parameters which approximate the pore oscillation behaviour.

For a cylindrically shaped pore the frictional term can be deduced from the Hagen-Poiseuille law of flow resistance through a capillary. There the frictional force F_R is proportional to the volume flow $\frac{\partial V}{\partial t}$ according to

$$F_R = A \cdot \Delta p = A \cdot \frac{\partial V}{\partial t} \cdot R \quad (11)$$

with the capillary cross section A and the flow resistivity

$$R = \frac{8\mu l}{\pi r^4} \quad (12)$$

On the other hand, for the oscillator the frictional force is

$$F_R = b \frac{\partial z}{\partial t} \quad (13)$$

Combining Eqs. 11,12 and 13 leads to

$$b \frac{\partial z}{\partial t} = A \cdot \frac{\partial V}{\partial t} \cdot \frac{8\mu l}{\pi r^4} = A \cdot A \cdot \frac{\partial z}{\partial t} \cdot \frac{8\mu l}{\pi r^4} = A \cdot \frac{\partial z}{\partial t} \cdot \frac{8\mu l}{r^2} \quad (14)$$

and therefore

$$\frac{b}{m} = \frac{1}{\rho_L A l} A \cdot \frac{\partial z}{\partial t} \cdot \frac{8\mu l}{r^2} = \frac{8\mu}{r^2 \rho_L} \quad (15)$$

In case of a tapered tube, this value has to be corrected for the energy required by the radial displacement of the liquid flowing through the capillary. However, due to the symmetric tapered shape of the bi-conical pore this correction cancels out for a full oscillation cycle of the fluid along the z-direction, but the average radius has to be adjusted to about $r/2$ for a nearly saturated pore. The dependence of the frictional term of the linear harmonic oscillator in the case of a saturated bi-conical pore can therefore be written as

$$\frac{b}{m} = \frac{32\mu}{r^2 \rho_L} \quad (16)$$

The comparison of the resonance frequency and the frictional term between the "straight forward" linear oscillator (LO), where parameter values from Tab. 1 have been used, and the average fit of a linear oscillator to the Navier stokes calculations (LONS) using the same parameter values is shown in Tab. 3.

	LO	LONS
1mm		
resonance frequency [Hz]	2.76	5.5
frictional term b/m [N s m ⁻¹ kg ⁻¹]	24	3.2
3mm		
resonance frequency [Hz]	0.53	1.4
frictional term b/m [N s m ⁻¹ kg ⁻¹]	2.7	1.2
3mm, low viscosity		
resonance frequency [Hz]	0.53	1.8
frictional term b/m [N s m ⁻¹ kg ⁻¹]	0.27	1.0

Table 3 : Comparison of resonance frequency and frictional terms between the linear oscillator (LO) and the average fit of a linear oscillator to the Navier Stokes calculations (LONS)

The resonance frequencies of the LONS are consistently about a factor of 2 larger than for the LO. However, they compare well within the same order of magnitude also for different pore sizes. Therefore Eq. 4 appears to be a good approximation which could even be improved by an "empirical factor" of 2.

Regarding the frictional term, the approximation (Eq. 16) gives the right order of magnitude, but for the LONS the dependence on viscosity is much less than for the LO.

Observation of the signals at the surface

In order to explore the feasibility of the explanation by pore level oscillations, the following approximation is made.

Assuming frequency dependent forces in the order of a fraction c of the capillary forces for each pore, the measured velocity at the earth surface due to the coherent oscillations of the pores in the hydrocarbon containing porous layer of thickness d at depth D as indicated in Fig. 11 can be estimated.

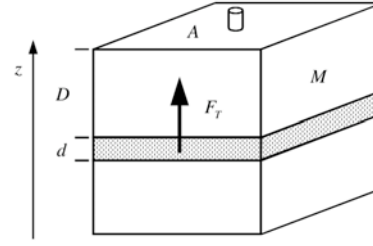


Figure 11 : Simple model for the occurrence of low frequency seismic signals due to pore liquid oscillations. At the surface a seismic sensor measures the surface motion.

The total force F_T represents the coherent sum of the fractional forces of the n pore oscillators

$$F_T = n F_z,$$

$$n = \frac{3\eta d A}{2r^2 \pi h}, \quad (17)$$

$$F_z = c \cdot \gamma \cdot 2\pi r \sin(\omega t)$$

This force accelerates the mass $M = D A \rho_R$ of the overlying rock material according to Newton's law

$$F_T = M \frac{\partial^2 z}{\partial t^2} \quad (18)$$

which leads to a measurable velocity at the earth surface on top of the reservoir of

$$\frac{\partial z}{\partial t} = -\frac{n}{M\omega} c \cdot \gamma \cdot 2\pi r \cos(\omega t) = -v_z \cos(\omega t) \quad (19)$$

The value

$$v_z = \frac{n}{M\omega} c \cdot \gamma \cdot 2\pi r = \frac{3\eta d c \gamma}{r h \omega D \rho_R} \quad (20)$$

is compatible with typical measured values of the vertical component of the ground velocity of about 10^{-6} m s⁻¹ for the realistic parameter values listed in Tab. 4.

The parameter c represents the fraction of the capillary force which is assumed to contribute to the total force which produces measurable signals at the surface. The value of c has to be compared to the frequency dependent forces calculated by the Navier Stokes Equations (Fig. 9) : the "triple line

force" and the "inertia", which are the same forces phase shifted by half an oscillation period (Fig. 8). The difference of these forces between "on" and "off" resonance is about 10% of the total force. The value of $c=10^{-2}$ therefore represents a rather conservative estimation which could be chosen closer to $c=10^{-1}$.

depth of hydrocarbon containing formation	D	10^3	m
hydrocarbon layer thickness	d	20	m
density of rock material	ρ_R	$2 \cdot 10^3$	kg m^{-3}
porosity	η	0.2	
fraction of maximum capillary force at ORCL= $2 \cdot \pi \cdot r$	c	10^{-2}	

Table 4: Common parameter values for reservoir structure.

Nonlinear oscillation due to a spherical pore shape

As the initial example has shown the explanation of the fine structure wiggles shown in Fig. 1 may be explained by the occurrence of non-linearity in the above model by allowing for a more general pore shape, e.g. spherical as shown in Fig. 12. This defines a more general, non-linear spring constant in a natural way. Such nonlinearities actually provide the more common case in nature ([9] and references to Oh and Shatterly 1979 and Payatakes et al 1980 therein).

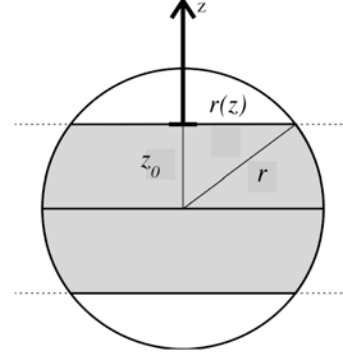


Figure 12: Schematic representation of a spherical pore geometry which enables low frequency oscillations of the contained liquid along the z-direction. Similar to the bi-conical case shown in Fig. 3, the liquid surface boundary forms the oil/rock contact line and the restoring capillary forces drive the liquid back along the z-direction towards its equilibrium position after an initial dislocation. While the bi-conical pore geometry leads to a linear spring constant for the restoring motion, the spherical pore geometry results in a non-linear spring constant that depends on the dislocation and therefore leads to a non-linear restoring motion.

The non-linear spring constant depending on the filling level z_0 is given by

$$f = \frac{\partial}{\partial z}(\gamma 2\pi(z)) = 2\pi\gamma \frac{\partial}{\partial z} \sqrt{r^2 - (z_0 + z)^2} = -\frac{2\pi\gamma(z_0 + z)}{\sqrt{r^2 - (z_0 + z)^2}} \quad (21)$$

which leads to the non-linear one-dimensional differential equation

$$\frac{\partial^2 z}{\partial t^2} + \frac{b}{m} \frac{\partial z}{\partial t} + \frac{2\pi\gamma(z_0 + z)z}{m\sqrt{r^2 - (z_0 + z)^2}} = \frac{F_0}{m} \cos(\omega t) \quad (22)$$

The filling-level dependent oscillation mass and frequency are

$$m = \frac{4}{3} \pi r^3 \rho_L \frac{(3r^2 z_0 - z_0^3)}{2r^3} \quad (23)$$

and

$$\omega_0 = \sqrt{f/m} \approx \sqrt{\frac{2\pi\gamma z_0}{m\sqrt{r^2 - z_0^2}}} \quad (24)$$

The synthetic spectra obtained from the nonlinear model are displayed in Fig. 13 for different filling levels. The single peak

spectrum of the linear case splits up into several peaks which are separated by the driving oscillation frequency.

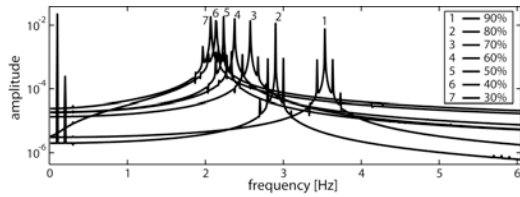


Figure 13: Spectrum of nonlinear oscillations in a spherical pore for different oil saturations. Pore liquid filling levels z_0 are between 0.3 and 0.9. The frequency spacing of the multiple peaks is a typical feature of nonlinear systems and corresponds to the frequency of the driving oscillation at 0.1 Hz, which also produces its own overtone at 0.2 Hz. For demonstration reasons, the damping was set to zero which leads to sharper peaks.

The frequency of the spectrum shifts toward larger values as the oil saturation increases. Note that these features need a certain transient time to build up, as is demonstrated in Fig. 14.

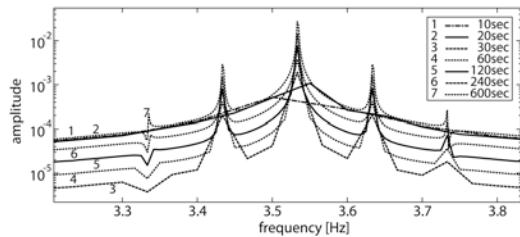


Figure 14: Development of the spectrum of nonlinear oscillations in a spherical pore during 600 s for filling level $z_0 = 0.9$ of the pore liquid. The frequency spacing of the multiple peaks is a typical feature of nonlinear systems and corresponds to the frequency of the driving oscillation at 0.1 Hz.

Natural oscillation frequency of pore: $\nu = 3.527$ Hz, mass of liquid in pore $m = 2.64 \cdot 10^{-5}$ kg.

If Eq. 22 is transformed into Eq. 1 by approximating the third term on the left hand side by a Taylor series, the coefficients A and B can be compared. It turns out that arbitrarily large values can be created by the variation of z_0 and r , since their difference appears in the denominators

of both coefficients. The spherical shape of pores is therefore a valuable candidate for a model explaining the observation displayed in Fig. 1. However, the assumption of a linear frictional term has to be analyzed in more detail in order to cover additional possible nonlinearities.

Discussion

The observed oscillations seem to commonly appear in the low frequency range between 1 and 10 Hz at all investigated sites independent of the hydrocarbon reservoir thickness. This favours the microscopic oscillator model compared to a reservoir thickness dependent macroscopic resonator model. In order to obtain sufficiently low resonance frequencies the "spring constant" has to be small which requires a low value of the surface tension γ , a large oscillating mass and a large value of the aspect ratio h/r . Surface tension and interfacial tension values in pore media are not well investigated [9] but can be orders of magnitude lower than the literature values of water ($73 \cdot 10^{-3}$ N/m) or crude oil ($20 \cdot 10^{-3}$ N/m) due to contamination, increased temperatures and contact of the oil to water as an additional liquid medium in the pores. Water wetted pore surfaces also lower interfacial tension and avoid pinning effects of the ORCL [9]. A large oscillating mass requires large pore diameters or the coupling of several smaller pores.

The assumption of coherent superposition of frictional forces requires either spatially coherent excitation (e.g. by the strong long-wavelength oceanic wave component of the geological background noise spectrum) or a coherent coupling mechanism between the pores either through the liquid or the solid phases. In the case of low frequency oceanic wave excitation this assumption is well satisfied. The coupling of the pore level oscillations to the rock material and the propagation of the seismic wave to the surface is presently under investigation. Also other effects that may create similar

signals, e.g. such as trapping of surface waves in near surface geological structures [11] are the subject of extensive numerical modelling

Conclusions

It has been shown that the phenomenological model of a driven one-dimensional linear and nonlinear oscillator can provide a natural interpretation of characteristic spectral features empirically attributable to hydrocarbon reservoirs. The basic requirement for oscillations, the presence of a restoring force on the pore scale, has been derived from first principles using Navier-Stokes Equations. Good agreement between the numerical results and the observations is achieved for realistic parameter values using the dominant part of the ever present background wave spectrum, the seismic wave field around 0.1-0.2 Hz caused by oceanic waves, as the driving force for the oscillations.

Acknowledgements

We thank Stefan Schmalholz, Department of Earth Sciences, ETH Zurich, Switzerland and Yuri Podladchikov, Physics of Geological Processes, University of Oslo, Norway for their fruitful discussions and suggestions.

References

- [1] R. Holzner, P. Eschle, H. Zürcher, M. Lambert, R. Graf, S. Dangel, P.F. Meier "Applying microtremor analysis to identify hydrocarbon reservoirs" *First Break* **23** (2005) 41-49
- [2] HyMAS is a trade mark of Spectraseis Technologie AG, Switzerland
- [3] S. Dangel et al "Phenomenology of tremor-like signals observed over hydrocarbon reservoirs", *Journal of Volcanology and Geothermal Research* **128** (2003) 135-158
- [4] A. Al Dulaijan, P. Van Mastrigt, F. Al-Somali, K.Saadaoui, I. Morris, "New Technology Applications in the Rub Al-Khali Desert, Proceedings of "GEO 2006 Middle East Conference and Exhibition", Bahrain, March 27-29, 2006
- [5] G. Rached, (Presentation A27), "Surface Passive Seismic Measurements In Kuwait", A.E. Suntsov, S.L. Aroutunov, A.M. Mekhnin, B.Y. Meltchouk, (Presentation A25), "Passive Infra-Frequency Microseismic Technology – Experience and Problems of Practical Use" K. Akrawi, G. Bloch (Presentation A28), "Application of Passive Seismic (IPDS) Surveys in Arabian Peninsula" O.L. Kouznetsov, I.A. Chirkine, A.V. Volkov, B.Y. Meltchouk, A.S. Vorobiev , A.S. Joukov, G.V. Rogotsky, K.Z. Sydykov (Presentation A36) "Applying Seismic Location of Emission Centers (Slec) to Monitor the Production in Oil-and-Gas Fields" Proceedings of "EAGE Workshop "Passive Seismic: Exploration and Monitoring Applications", Dubai, United Arab Emirates, 10 - 13 December 2006
- [6] O.L. Kuznetsov, B.M. Grafov, S.L. Aroutunov, A.E. Suntsov, "About the theory of ANCHAR method", in *Geofizika special issue (in Russian) "Seismic Exploration Technologies II"*, (2003)103-107
- [7] I. Macedo, R. Dittz, A. Santos de Oliveira, R. Holzner, R.Graf "Observation and modeling of seismic background noise" Ninth International Congress of the Brazilian Geophysical Society, 11-14 September 2005, Salvador - Bahia, Brazil.
- [8] R. Holzner, P. Eschle, P.F. Meier, S. Dangel, "Linear Model for low frequency pore liquid oscillations observed in Hydrocarbon Microtremor Analysis (HyMAS)", *GEO 2006*, 27-29 March 2006, Bahrain R. Holzner, P. Eschle, M. Frehner, S. Schmalholz, Y. Podladchikov, "Hydrocarbon Microtremors interpreted as Nonlinear Oscillations Driven by Oceanic Background Waves", EAGE 68th Conference & Exhibition, Vienna, Austria, 12 - 15 June 2006
- [9] M. Hilpert et al "Capillarity-induced resonance of oil blobs in capillary tubes and porous media" *Geophysics* **65** (2000) 874-883
- [10] TransAT is a protected trademark: www.ascomp.ch/transat.html
- [11] Cinna Lomnitz and Yunny Meas "Huygens' Principle: The capture of seismic energy by a soft soil layer", *Geophys. Res. Lett.* **31**(2004)L13613